

## Supplementary Information

### Surface plasmon resonance and structure defects synergistic effect of ZnCdS<sub>2</sub>/NiMoO<sub>4</sub>@Cu Z-scheme heterojunction for enhanced photocatalytic CO<sub>2</sub> reduction to CH<sub>4</sub>

Zhentao Hu,<sup>a</sup> Lei Huang,<sup>a</sup> Bojing Sun,<sup>\*a,b</sup> Dongfang Hou,<sup>\*a,b</sup> Xiu-qing Qiao,<sup>a,b</sup> Meidi Wang,<sup>a,b</sup> Huijuan Ma,<sup>b</sup> and Dong-Sheng Li<sup>\*a,b</sup>

<sup>a</sup> College of Materials and Chemical Engineering, Key Laboratory of Inorganic College of Materials and Chemical Engineering, Key Laboratory of Inorganic Nonmetallic Crystalline and Energy Conversion Materials, China Three Gorges University, Yichang, Hubei 443002, P.R. China

<sup>b</sup> Hubei Three Gorges Laboratory, Yichang, Hubei 443007, P. R. China

E-mail: [sunbojing@ctgu.edu.cn](mailto:sunbojing@ctgu.edu.cn) (Bojing Sun); [dfhouok@126.com](mailto:dfhouok@126.com) (Dongfang Hou); [lidongsheng1@126.com](mailto:lidongsheng1@126.com) (Dong-sheng Li).

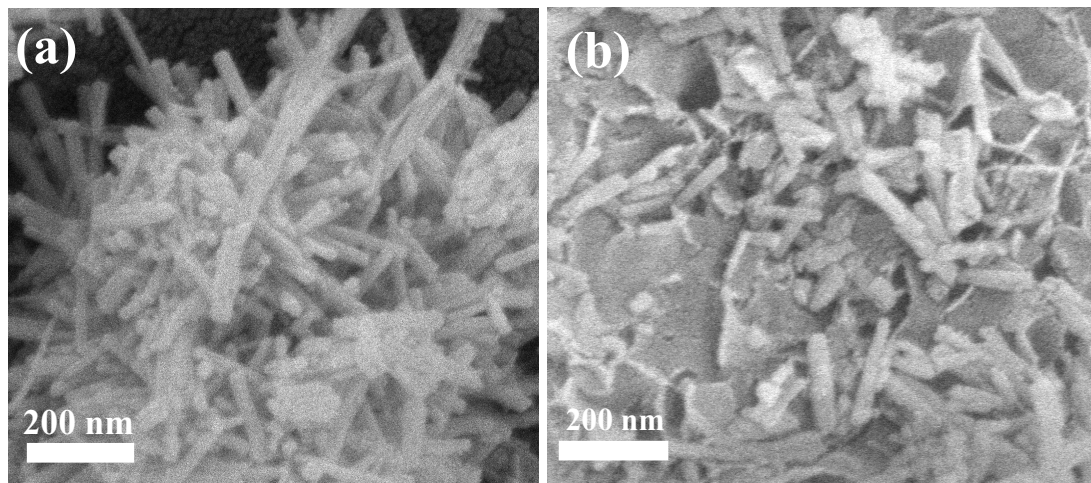


**Fig. S1. a-b** The SEM images of ZCS and ZCS/NMO.

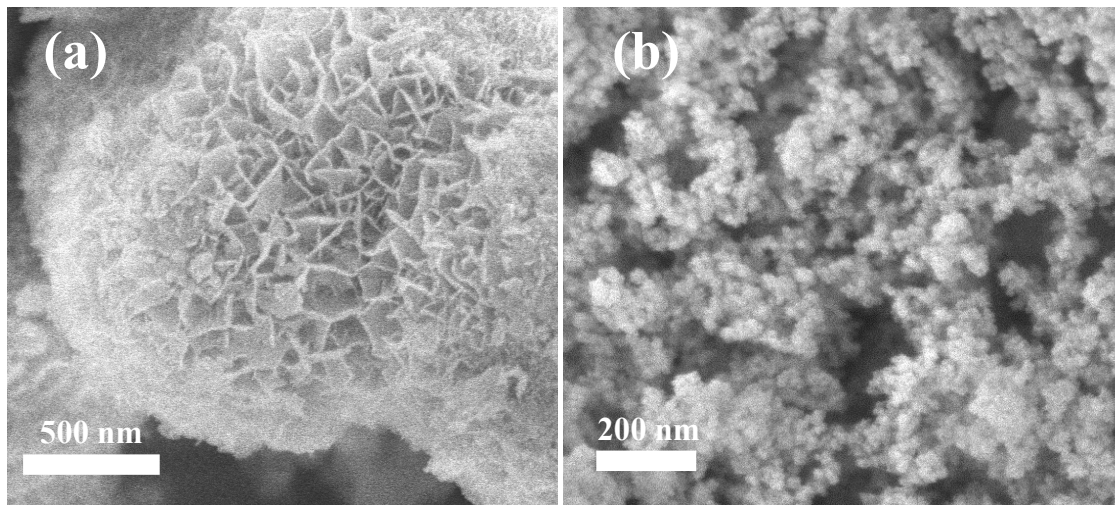


**Fig. S2. a-b** The SEM images of  $\text{NiMoO}_4$  and Cu.

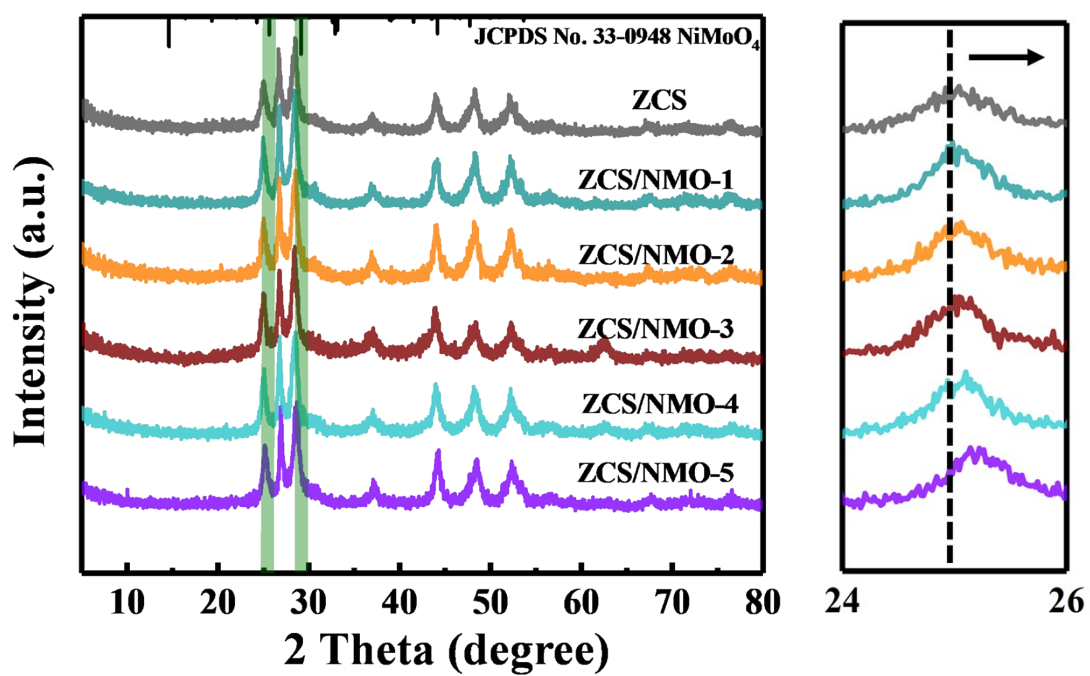


**Fig. S3.** The XRD patterns and magnified patterns of ZCS and ZCS/NMO-X

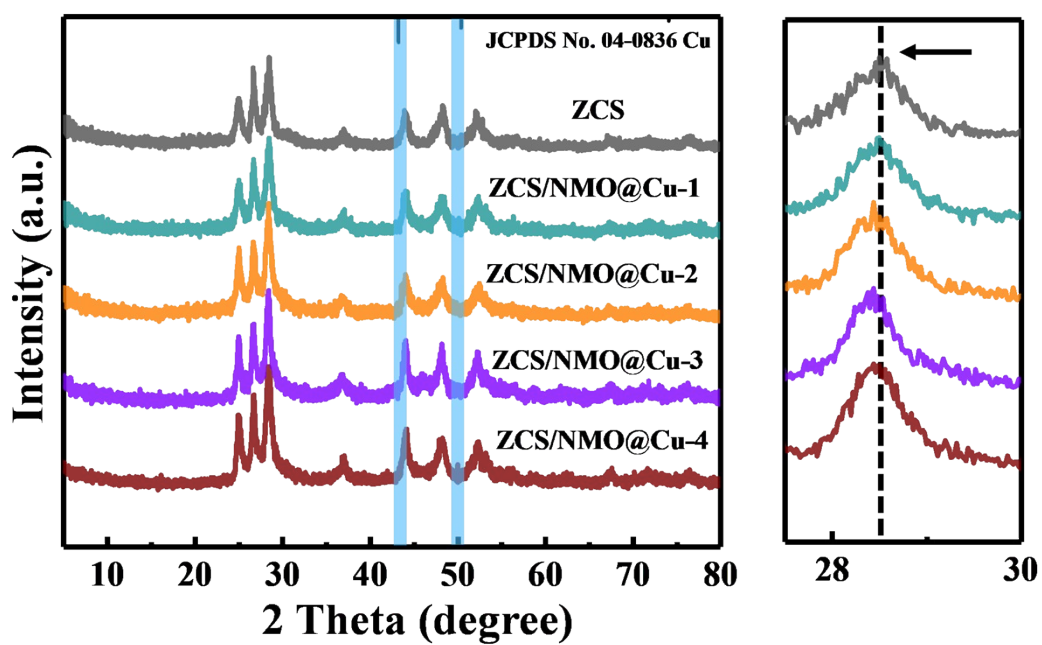


**Fig. S4.** The XRD patterns and magnified patterns of ZCS and ZCS/NMO@Cu-X

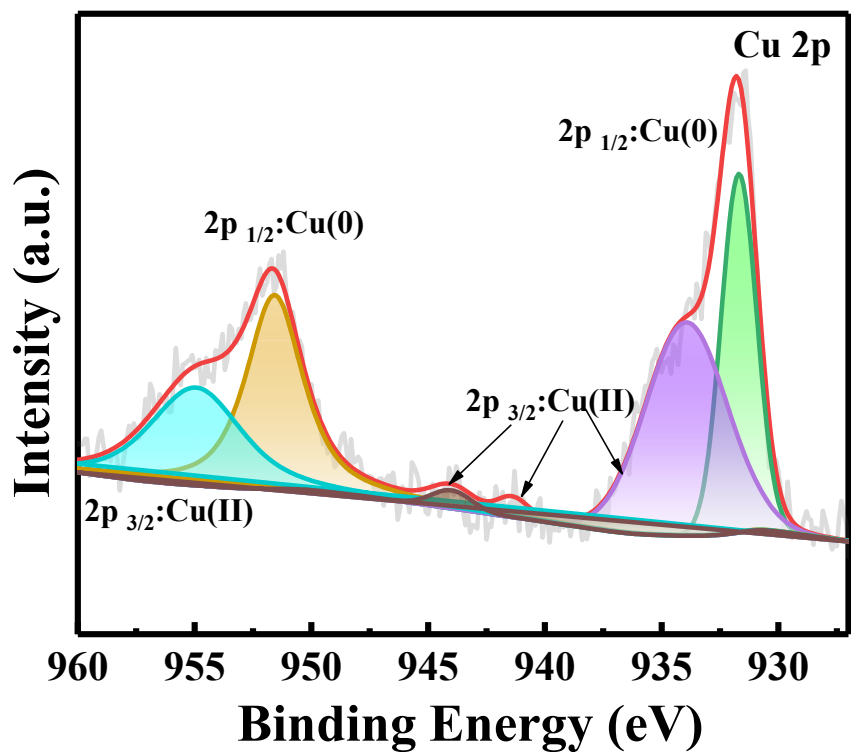


**Fig. S5.** High resolution XPS spectra of Cu 2p of ZCS/NMO@Cu

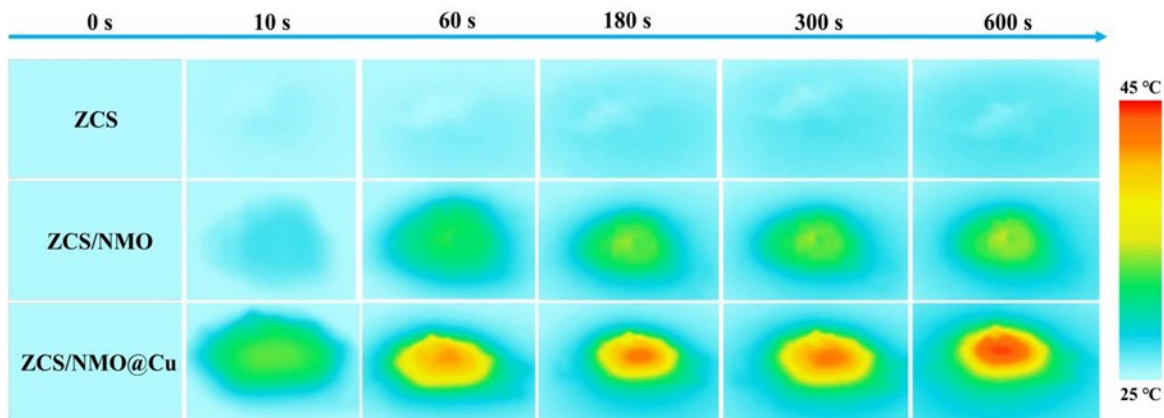


**Fig. S6.** Photothermal maps of ZCS, ZCS/NMO, and ZCS/NMO@Cu under near-infrared light irradiation at different times.

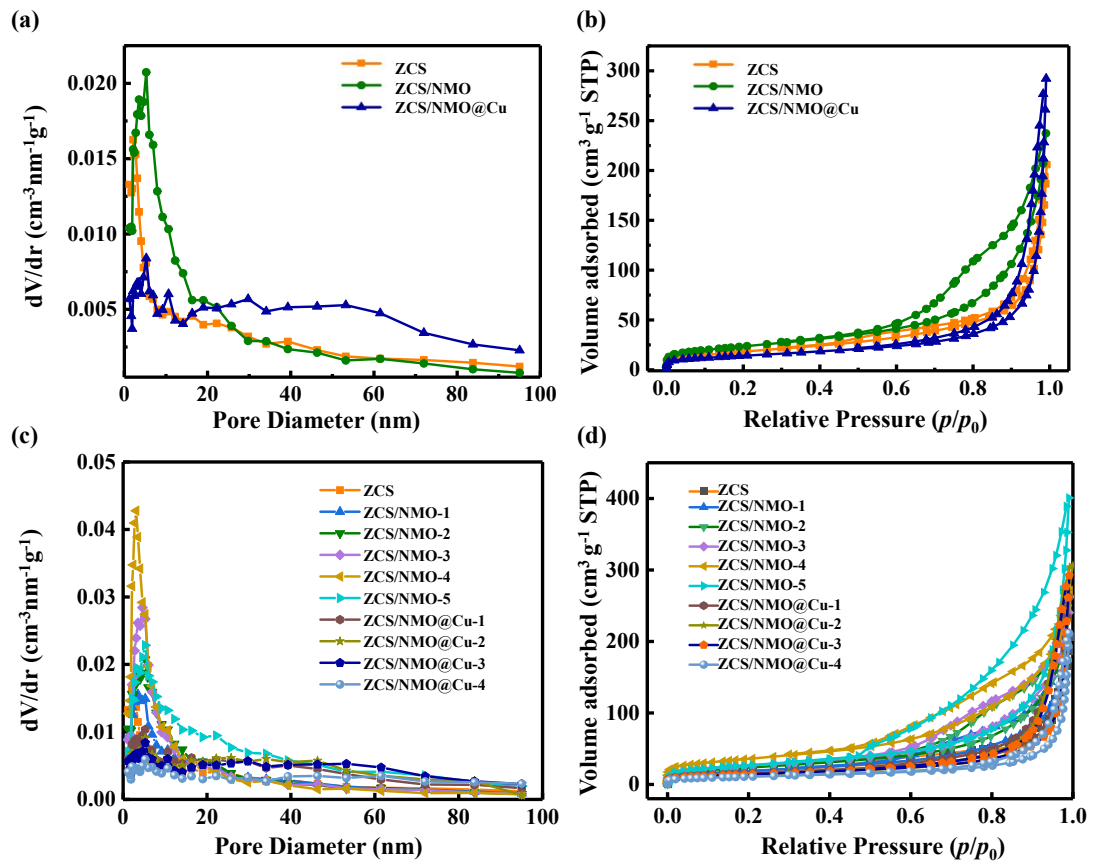


**Fig. S7.** **a** Pore size distribution of ZCS, ZCS/NMO and ZCS/NMO@Cu. **b** Nitrogen sorption isotherms of ZCS, ZCS/NMO and ZCS/NMO@Cu. **c** Pore size distribution of ZCS, ZCS/NMO-X and ZCS/NMO@Cu-X. **d** Nitrogen sorption isotherms of ZCS, ZCS/NMO-X and ZCS/NMO@Cu-X.

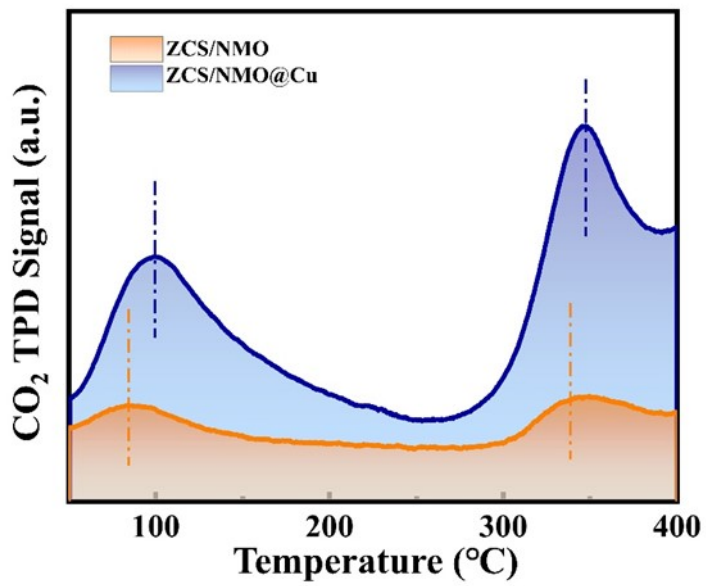


**Fig. S8.** CO<sub>2</sub> TPD profiles of ZCS/NMO and ZCS/NMO@Cu.

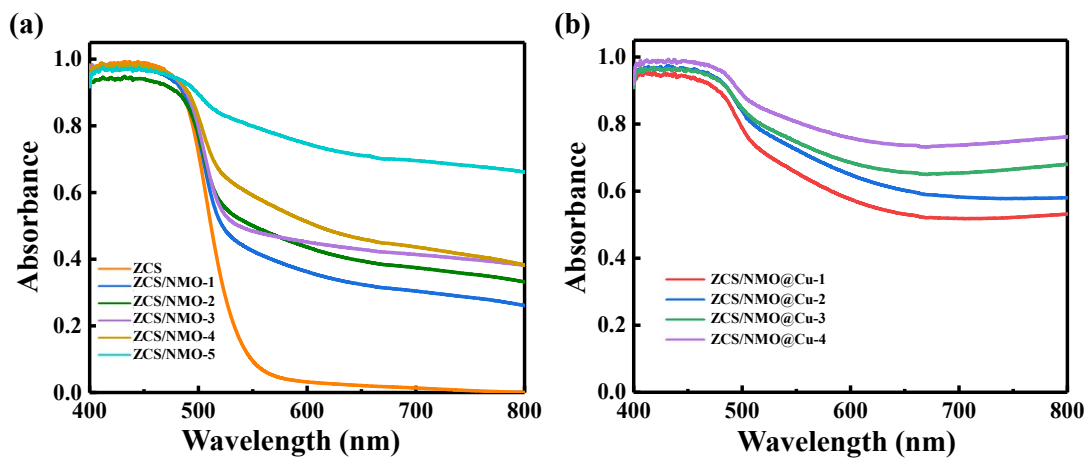


**Fig. S9.** **a** UV-vis absorption spectra of ZCS and ZCS/NMO-X. **b** UV-vis absorption spectra of ZCS/NMO@Cu-X

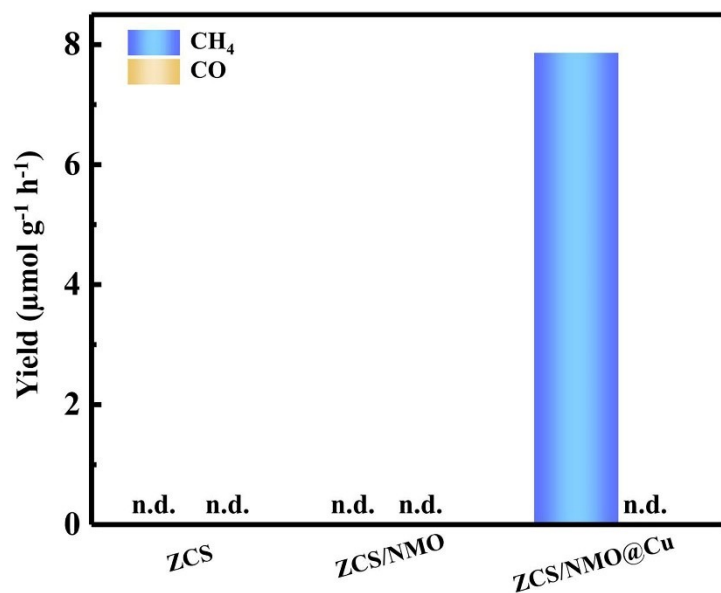


**Fig S10.** CO<sub>2</sub> reduction performance under near-infrared light irradiation.

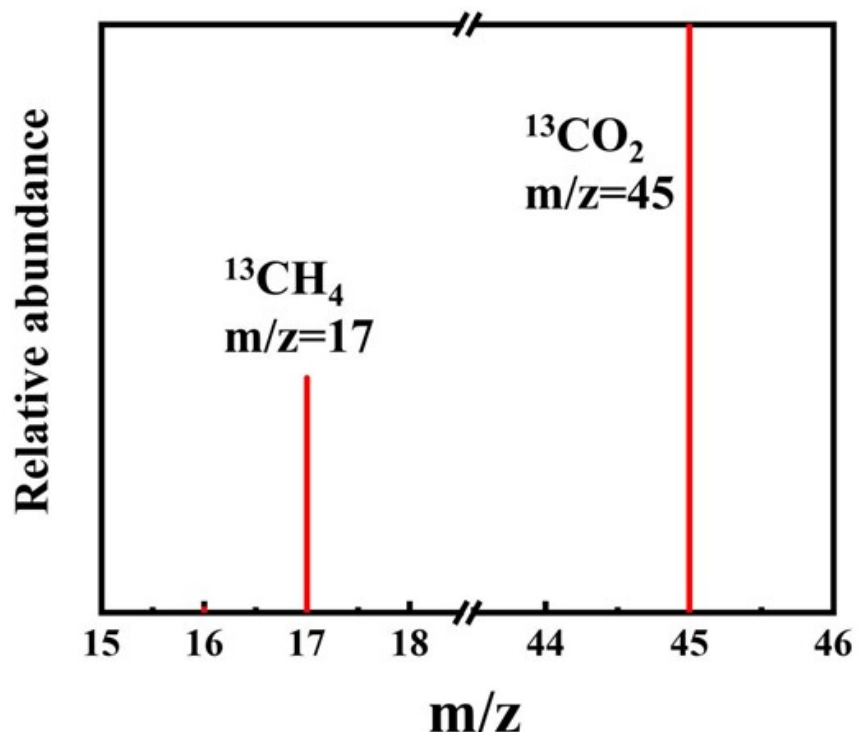


**Fig S11.** Mass spectra of  $^{13}\text{CH}_4$  generated from the isotopic  $^{13}\text{CO}_2$  photoreduction.

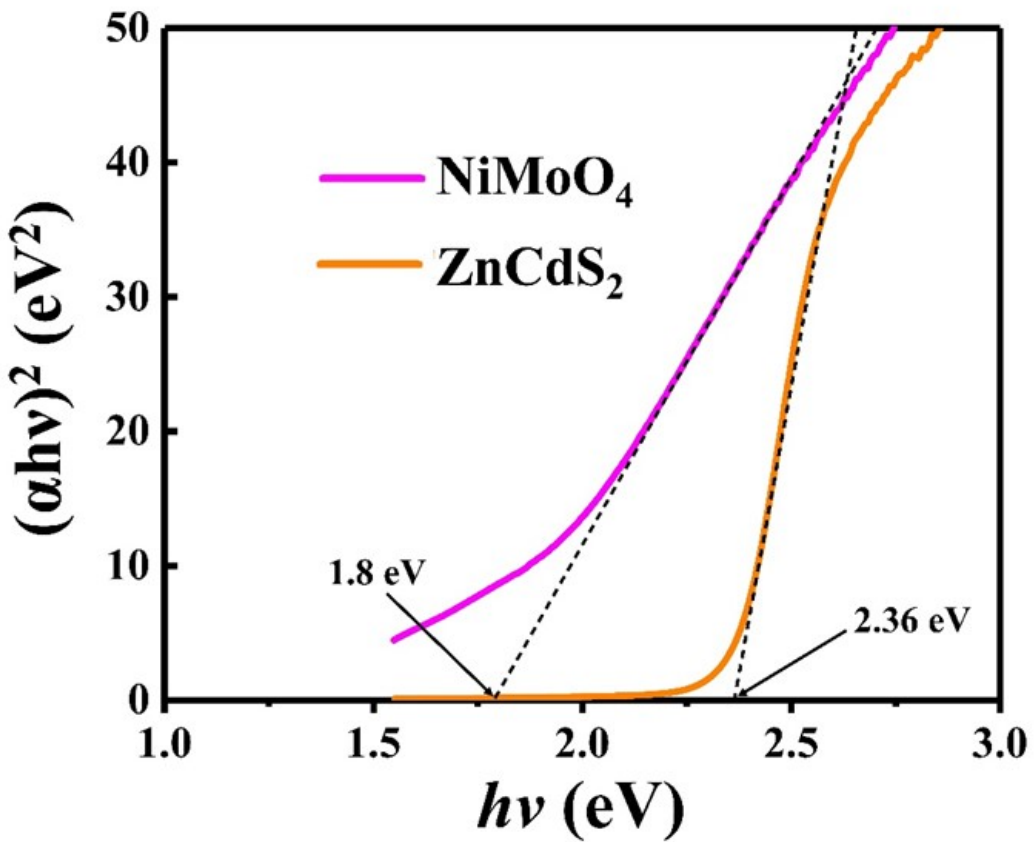


**Fig S12.** Band gap spectra of  $\text{ZnCdS}_2$  and  $\text{NiMoO}_4$ .

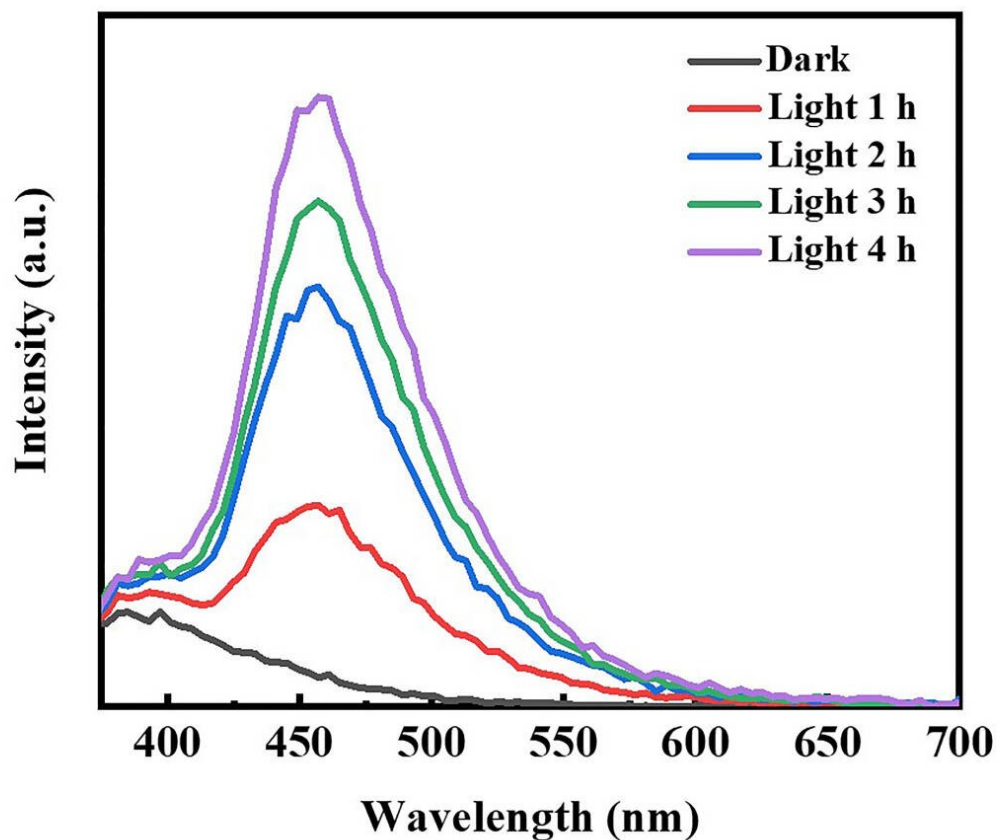


**Fig S13.** Fluorescence spectra of ZCS/NMO@Cu under visible irradiation.

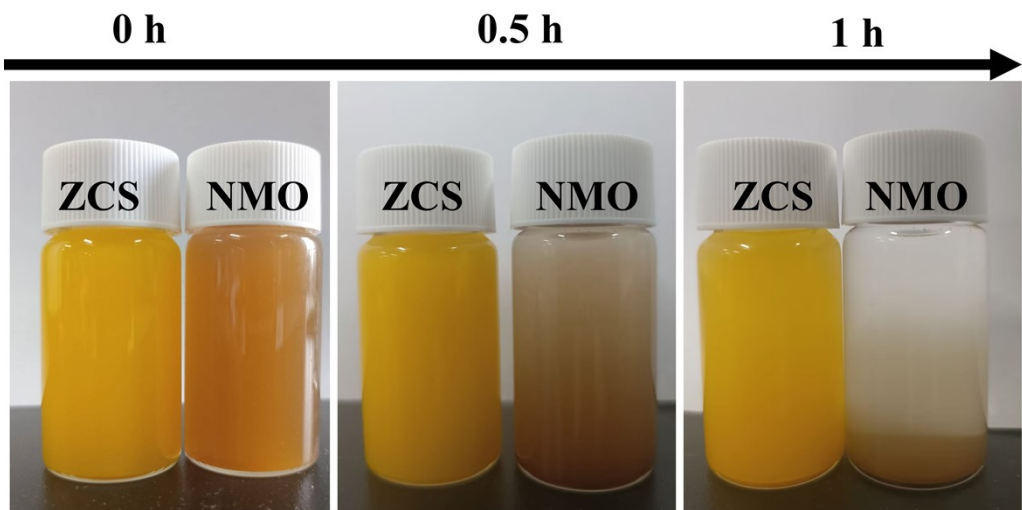


**Fig S14.** Static experiment of ZCS and NMO.

**Table S1** Specific surface areas and pore volume of ZCS, ZCS/NMO-X and ZCS/NMO@Cu-X.

Sample	Surface area (m <sup>2</sup> /g)	Mean pore diameter (nm)	Pore volume (cm <sup>3</sup> /g)
ZCS	<b>68.43</b>	<b>17.10</b>	<b>0.29</b>
ZCS/NMO-1	<b>68.6</b>	<b>18.82</b>	<b>0.32</b>
ZCS/NMO-2	<b>85.45</b>	<b>17.10</b>	<b>0.37</b>
ZCS/NMO-3	<b>95.05</b>	<b>15.71</b>	<b>0.37</b>
ZCS/NMO-4	<b>128.97</b>	<b>12.48</b>	<b>0.40</b>
ZCS/NMO-5	<b>97.7</b>	<b>25.15</b>	<b>0.61</b>
ZCS/NMO@Cu-1	<b>56.19</b>	<b>28.71</b>	<b>0.40</b>
ZCS/NMO@Cu-2	<b>49.11</b>	<b>34.56</b>	<b>0.42</b>
ZCS/NMO@Cu-3	<b>51.29</b>	<b>34.05</b>	<b>0.44</b>
ZCS/NMO@Cu-4	<b>38.46</b>	<b>32.79</b>	<b>0.32</b>

**Table S2** Comparison of photocatalytic CO<sub>2</sub> conversion to CH<sub>4</sub> performance of our photocatalysts with previously reported system of similar catalytic materials.

Catalyst	Light Source	CH <sub>4</sub> yield	Selectivity	Ref
UiO-66/Co <sub>9</sub> S <sub>8</sub>	300W Xe lamp, AM 1.5	240.9 μmol·g <sup>-1</sup> ·h <sup>-1</sup>	~100%	1
CuSnInS <sub>4</sub>	300W Xe lamp, >420 nm	5.83 μmol·g <sup>-1</sup> ·h <sup>-1</sup> ,	67.3%	2
Vs-CuIn <sub>5</sub> S <sub>8</sub>	300W Xe lamp, >420 nm	8.7 μmol·g <sup>-1</sup> ·h <sup>-1</sup> ,	~100%	3
Bi <sub>2</sub> WO <sub>6</sub> /ZnIn <sub>2</sub> S <sub>4</sub>	300W Xe lamp, >420 nm	5.12 μmol·g <sup>-1</sup> ·h <sup>-1</sup> ,	94.5%	4
C <sub>60</sub> /CuS@ZnIn <sub>2</sub> S <sub>4</sub>	300W Xe lamp (>400 nm), H <sub>2</sub> O	43.6 μmol·g <sup>-1</sup> ·h <sup>-1</sup> ,	~100%	5
ZnIn <sub>2</sub> S <sub>4</sub> /N-doped graphene	300W Xe lamp, >420 nm	1.01 μmol·g <sup>-1</sup> ·h <sup>-1</sup>	42.4%	6
TiO <sub>2</sub> -Cu <sub>2</sub> ZnSnS <sub>4</sub>	400 W Xe lamp, ≥420 nm	1.01 μmol·g <sup>-1</sup> ·h <sup>-1</sup>	0.05%	7
Cu-ZnIn <sub>2</sub> S <sub>4</sub> /ZIF-67	300W Xe lamp, 400-780 nm	22.27 μmol·g <sup>-1</sup> ·h <sup>-1</sup>	94.7%	8
NH <sub>2</sub> -B-TiO <sub>2</sub> - Cu <sub>x</sub> S	300W Xe lamp, >420 nm	3.34 μmol·g <sup>-1</sup> ·h <sup>-1</sup>	16%	9
BiOBr/CdIn <sub>2</sub> S <sub>4</sub>	300W Xe lamp, >420 nm	1.50 μmol·g <sup>-1</sup> ·h <sup>-1</sup>	16.7%	10
SnS <sub>2</sub>	150W halogen lamp, AM 1.5	0.13 μmol cm <sup>-2</sup>	92%	11

CuS@SnS <sub>2</sub>	300W Xe lamp, $\geq 400$ nm	77.5 $\mu\text{mol}\cdot\text{g}^{-1}\cdot\text{h}^{-1}$	35.6%	12
MoO <sub>3</sub> /MoS <sub>2</sub> /CuS	300W Xe lamp, $>420$ nm	44.64 $\mu\text{mol}\cdot\text{g}^{-1}\cdot\text{h}^{-1}$	85.5%	13
MoS <sub>2</sub> /SnS <sub>2</sub> /r-GO	8W mercury lamp, H <sub>2</sub> O	50.548 $\mu\text{mol}\cdot\text{g}^{-1}\cdot\text{h}^{-1}$	42.4%	14
In <sub>2</sub> S <sub>3</sub> /WS <sub>2</sub>	400W Xe lamp, $>420$ nm	16 $\mu\text{mol}\cdot\text{g}^{-1}\cdot\text{h}^{-1}$	47%	15
Co-ZnS/MoS <sub>2</sub> /graphene	350W Xe lamp, $>420$ nm	23.4 $\mu\text{mol}\cdot\text{g}^{-1}\cdot\text{h}^{-1}$	$\sim 100\%$	16
MS/In <sub>2</sub> S <sub>3</sub>	300W Xe lamp, $>420$ nm	68.41 $\mu\text{mol}\cdot\text{g}^{-1}\cdot\text{h}^{-1}$	80.3%	17
BiOI/MoS <sub>2</sub> /CdS	300W Xe lamp, $>420$ nm	46.22 $\mu\text{mol}\cdot\text{g}^{-1}\cdot\text{h}^{-1}$	55.6%	18
ZnFe <sub>2</sub> O <sub>4</sub> /ZnO/CdS	300W Xe lamp, $>420$ nm	105.9 $\mu\text{mol}\cdot\text{g}^{-1}\cdot\text{h}^{-1}$	28.5%	19
ZnCdS <sub>2</sub> /NiMoO <sub>4</sub> @Cu	300W Xe lamp, $>420$ nm	92.17 $\mu\text{mol}\cdot\text{g}^{-1}\cdot\text{h}^{-1}$	$\sim 100\%$	<b>This work</b>

**Table S3** Time-resolved fluorescence spectra of ZCS, ZCS/NMO-X and ZCS/NMO@Cu-X

Samples	$\tau_1$ (ns)	A <sub>1</sub>	$\tau_2$ (ns)	A <sub>2</sub>	$\tau$ (ns)
ZCS	<b>1.87</b>	<b>49.48</b>	6.33	<b>50.52</b>	<b>4.12</b>
ZCS/NMO	<b>0.85</b>	<b>18.83</b>	<b>4.17</b>	<b>81.17</b>	<b>3.55</b>
ZCS/NMO@Cu	<b>1.91</b>	<b>43.91</b>	<b>6.20</b>	<b>56.09</b>	<b>4.32</b>

- 1 S. Yang, W.J. Byun, F. Zhao, D. Chen, J. Mao, W. Zhang, J. Peng, C. Liu, Y. Pan, J. Hu, J. Zhu, X. Zheng, H. Fu, M. Yuan, H. Chen, R. Li, M. Zhou, W. Che, J.B. Baek, J.S. Lee, J. Xu, CO<sub>2</sub> Enrichment Boosts Highly Selective Infrared-Light-Driven CO<sub>2</sub> Conversion to CH<sub>4</sub> by UiO-66/Co<sub>9</sub>S<sub>8</sub> Photocatalyst, *Adv. Mater.* 2024, **36**, 2405825.
- 2 Y. Chai, Y. Kong, M. Lin, W. Lin, J. Shen, J. Long, R. Yuan, W. Dai, X. Wang, Z. Zhang, Metal to non-metal sites of metallic sulfides switching products from CO to CH<sub>4</sub> for photocatalytic CO<sub>2</sub> reduction, *Nat. Commun.* 2023, **14**, 4034
- 3 X. Li, Y. Sun, J. Xu, Y. Shao, J. Wu, X. Xu, Y. Pan, H. Ju, J. Zhu, Y. Xie, Selective visible-light-driven photocatalytic CO<sub>2</sub> reduction to CH<sub>4</sub> mediated by atomically thin CuIn<sub>5</sub>S<sub>8</sub> layers, *Nat. Energy.* 2019, **4**, 8, 690-699.
- 4 W. Yang, F. Zhou, N. Sun, J. Wu, Y. Qi, Y. Zhang, J. Song, Y. Sun, Q. Liu, X. Wang, J. Mi, M. Li, Constructing a 3D Bi<sub>2</sub>WO<sub>6</sub>/ZnIn<sub>2</sub>S<sub>4</sub> direct Z-scheme heterostructure for improved photocatalytic CO<sub>2</sub> reduction performance, *J. Colloid Interface Sci.* 2024, **622**, 695-706.
- 5 Y. Ding, Y. Chen, Z. Guan, Y. Zhao, J. Lin, Y. Jiao, G. Tian, Hierarchical CuS@ZnIn<sub>2</sub>S<sub>4</sub> Hollow Double-Shelled p-n Heterojunction Octahedra Decorated with Fullerene C<sub>60</sub> for Remarkable Selectivity and Activity of CO<sub>2</sub> Photoreduction into CH<sub>4</sub>, *ACS Appl. Mater. Interfaces* 2022, **14**, 7888-7899
- 6 Y. Xia, B. Cheng, J. Fan, J. Yu, G. Liu, Near-infrared absorbing 2D/3D ZnIn<sub>2</sub>S<sub>4</sub>/N-doped graphene photocatalyst for highly efficient CO<sub>2</sub> capture and photocatalytic reduction, *Sci China Mater* 2020, **63**, 4, 552–565.
- 7 A. Raza, H. Shen, A.A. Haidry, M.K. Shahzad, L. Sun, Facile in-situ fabrication of TiO<sub>2</sub>-Cu<sub>2</sub>ZnSnS<sub>4</sub> hybrid nanocomposites and their photoreduction of CO<sub>2</sub> to CO/CH<sub>4</sub> generation, *Appl. Surf. Sci.* 2020, **529**, 147005.
- 8 Z. Li, J. Xiong, Y. Huang, Y. Huang, G.I.N. Waterhouse, Z. Wang, Y. Mao, Z. Liang, X. Luo, Rational design of spatial charge separation and targeted active site Cu for highly selective photocatalytic CO<sub>2</sub> reduction to CH<sub>4</sub>, *Chem. Eng. J.* 2024, **495**, 153310.
- 9 Z. Chen, X. Zhu, J. Xiong, Z. Wen, G. Cheng, A p-n Junction by Coupling Amine-Enriched Brookite-TiO<sub>2</sub> Nanorods with Cu<sub>x</sub>S Nanoparticles for Improved Photocatalytic CO<sub>2</sub> Reduction, *Materials* 2023, **16**, 3, 960.
- 10 M. Shen, Y. Li, T. Luo, Z. Wang, M. Zhou, Y. Wang, S. Xu, Z. Li, In-situ construction of Bi-MOF-derived S-scheme BiOBr/CdIn<sub>2</sub>S<sub>4</sub> heterojunction with rich oxygen vacancy for selective photocatalytic CO<sub>2</sub> reduction using water, *Sep. Purif.* 2025, **355**, 129713.
- 11 T.T. Mamo, M. Qorbani, A.G. Hailemariam, R. Putikam, C.-M. Chu, T.-R. Ko, A. Sabbah, C.-Y. Huang, S. Kholimatussadiah, T. Billo, M.K. Hussien, S.-Y. Chang, M.-C. Lin, W.-Y. Woon, H.-L. Wu, K.-T. Wong, L.-C. Chen, K.-H. Chen, Enhanced CO<sub>2</sub> photoreduction to CH<sub>4</sub> via \*COOH and \*CHO intermediates stabilization by synergistic effect of implanted P and S vacancy in thin-film SnS<sub>2</sub>, *Nano Energy* 2024, **128**, 109863.
- 12 Y. Yin, Y. Chen, X. Yu, Q. Zhang, Y. Ru, G. Tian, The cooperative p-n heterojunction and Schottky junction in Au-decorated hierarchical CuS@SnS<sub>2</sub> hollow cubes for boosted charge transport and CO<sub>2</sub> photoreduction, *Chem. Eng. J.* 2024, **497**, 154713.
- 13 X. Zheng, Y. Li, H. Peng, J. Wen, Solar-light induced photoreduction of CO<sub>2</sub> using nonthermal plasma sulfurized MoO<sub>3</sub>@MoS<sub>2</sub>-CuS composites, *J. Environ. Chem. Eng.* 2021, **9**, 4, 105469.
- 14 S. Yin, J. Li, L. Sun, X. Li, D. Shen, X. Song, P. Huo, H. Wang, Y. Yan, Construction of Heterogenous S-C-S MoS<sub>2</sub>/SnS<sub>2</sub>/r-GO Heterojunction for Efficient CO<sub>2</sub> Photoreduction, *Inorg. Chem.* 2019, **58**, 15590–15601.
- 15 A.G. Alhamzani, T.A. Yousef, M.M. Abou-Krishna, K.Y. Kumar, M.K. Prashanth, L. Parashuram, B. Hun Jeon, M.S. Raghu, Fabrication of layered In<sub>2</sub>S<sub>3</sub>/WS<sub>2</sub> heterostructure for enhanced and efficient photocatalytic CO<sub>2</sub> reduction and various paraben degradation in water, *Chemosphere* 2023, **322**, 138235.
- 16 G.-J. Lee, Y.-H. Hou, H.-T. Huang, W. Wang, C. Lyu, J.J. Wu, Microwave-assisted solvothermal synthesis of chalcogenide composite photocatalyst and its photocatalytic CO<sub>2</sub> reduction activity under simulated solar light, *Catalysts* 2020, **10**, 7, 789.
- 17 W. Cai, Z. Qian, C. Hu, W. Zheng, L. Luo, Y. Zhao, Systematic investigation of MoS<sub>2</sub>-metal sulfides (Metal = In, Sn, Cu, Cd) heterostructure via metal-sulfur bond for photocatalytic CO<sub>2</sub> reduction, *Chem. Eng. J.* 2024, **479**, 147718.
- 18 Y. Li, H. Luo, Y. Bao, S. Guo, D. Lei, Y. Chen, Construction of Hierarchical BiOI/MoS<sub>2</sub>/CdS Heterostructured Microspheres for Boosting Photocatalytic CO<sub>2</sub> Reduction Under Visible Light, *Sol. RRL* 2021, **5**, 2100051.
- 19 B. Feng, Q. Wang, P. Liu, Z. Yuan, D. Pan, M. Ye, K. Shen, Z. Xin, Z-scheme heterojunction enhanced photocatalytic performance for CO<sub>2</sub> reduction to CH<sub>4</sub>, *Nanoscale* 2024, d4nr02897j.